

GRB 090227B: THE MISSING LINK BETWEEN THE GENUINE SHORT AND DISGUISED SHORT GRBS

M. MUCCINO^{1,2}, R. RUFFINI^{1,2,3}, C.L. BIANCO^{1,2}, L. IZZO^{1,2}, A.V. PENACCHIONI^{1,3}

Draft version April 3, 2019

ABSTRACT

The observational progress obtained by Fermi-GBM and Konus-Wind satellites is used to identify the new class of genuine short GRBs: short bursts with the same inner engine of the long GRBs but endowed with a severely low value of the Baryon load, $B \lesssim 5 \times 10^{-5}$. The emission from these GRBs mainly consists in a first emission, the P-GRB, followed by a softer emission “squeezed” on the first one. The typical separation between the two components is expected to be smaller than $10^{-3} - 10^{-2}$ s. Attention is given to the time-resolved spectral analysis of GRB 090227B. From the 16 ms time-binned light curves we find a significant thermal emission in the first 96 ms, which we identify with the P-GRB. The subsequent emission is identified with the extended afterglow. We find a P-GRB with the highest temperature ever observed, $kT = 517$ keV. We estimate from our theoretical model the cosmological redshift $z = 1.61$ and, consequently, we derive the total energy $E_{e^+e^-}^{\text{tot}} = 2.83 \times 10^{53}$ ergs, the Baryon load $B = 4.13 \times 10^{-5}$, the Lorentz Γ factor at transparency $\Gamma_{tr} = 14365$, and the intrinsic duration $\Delta t' \sim 0.35$. We also determine the average density of the CircumBurst Medium (CBM), $\langle n_{CBM} \rangle = 1.9 \times 10^{-5}$ particles/cm³. There is no evidence of beaming in the system. In view of the energetics and of the Baryon load of the source, as well as of the low interstellar medium and of the intrinsic time scale of the signal, we identify the GRB progenitor as a binary neutron star. From the recent developed theory of the neutron stars configuration, we estimate the masses of the stars, $m_1 = m_2 = 1.34M_{\odot}$, their radii, $R_1 = R_2 = 12.24$ km, and the thickness of their crusts, ~ 0.47 km, consistent with the above values of the Baryon load, of the energetics and of the time duration of the event.

Subject headings: Gamma-ray burst: general — Gamma-ray burst: individual: GRB 090227B

1. INTRODUCTION

The understanding of GRBs is among the most fascinating and profound conceptual problems of relativistic astrophysics. Observations at high energies from space missions, such as BATSE (Meegan et al. 1992), Beppo-SAX (Metzger et al. 1997), Swift Burst Alert Telescope (BAT) (Gehrels et al. 2005), AGILE (Tavani et al. 2008), Fermi Gamma-ray Burst Monitor (GBM) (Meegan et al. 2009) and others, have revealed that GRBs emit in a few seconds of the time of the observer almost the energy equivalent to a solar mass. This allows the observability of these sources over the entire visible Universe.

The first systematic analysis on a large sample of GRBs was made possible by the BATSE instrument on board the Compton Gamma-Ray Observer (CGRO) satellite (Meegan et al. 1992). One of the main outcomes of this early analysis was the evidence of a bi-modal temporal distribution in the T_{90} observed duration of prompt emission of GRBs. The T_{90} duration is defined as the time interval over which 90% of the total background-subtracted counts are observed, with the interval starting when 5% of the total counts have been observed. The “long” and “short” GRBs were defined as being longer or shorter than $T_{90} = 2$ s. The observed spectra of the “short” GRBs have appeared also to be systematically harder than the ones of the “long” (Klebesadel 1992; Dezalay et al. 1992; Kouveliotou et al. 1993; Tavani 1998). This dichotomy led to an idea of different progenitors: respectively, the explosion of very massive stars for long GRBs (see e.g. the collapsar

model by Woosley 1993) and the merger of compact objects for short GRBs (Blinnikov et al. 1984; Paczynski 1998). This classification and associated quest for progenitors was clearly premature, both from an observational and theoretical point of view, with a lack of understanding of some fundamental parameters. It is sufficient to say that the cosmological nature of these sources had not yet been established.

After BATSE, a fundamental progress was achieved with the discovery by Beppo-SAX of a prolonged soft X-ray emission, following the traditional hard X-ray emission observed by BATSE (Costa et al. 1997). The Beppo-SAX observed soft X-ray emission, lasting from few days to months, was named the “afterglow”, while the BATSE observations were referred as the “prompt emission”. The afterglow allowed to pinpoint more accurately the GRB position in the sky with narrow field instruments and permitted the identification of their optical counterpart by space and ground based telescopes. This has allowed to measure their redshift, confirming their cosmological nature (van Paradijs et al. 1997).

In recent years, the observations by Swift satellite (Gehrels et al. 2005) evidenced the existence of a possible third class of burst presenting hybrid properties between the short and the long ones: the Norris-Bonnell sources (Norris & Bonnell 2006). The prompt emission of these sources is characterized by an initial short spike-like emission lasting a few seconds, followed by a prolonged softer extended emission lasting up to some hundred seconds. They were initially indicated in the literature as “short GRBs with an extended emission”.

In parallel the theoretical progress in the Fireshell model of GRBs (see Ruffini et al. 2001a,b,c) has led to an alternative explanation of the Norris-Bonnell sources as “disguised short bursts”: canonical long bursts exploding in a low density circum burst medium typical of galactic halos. In the Fireshell

¹ Dip. di Fisica and ICRA, Sapienza Università di Roma, Piazzale Aldo Moro 5, I-00185 Rome, Italy.

² ICRA Net, Piazza della Repubblica 10, I-65122 Pescara, Italy.

³ Université de Nice Sophia Antipolis, Nice, CEDEX 2, Grand Chateau Parc Valrose.

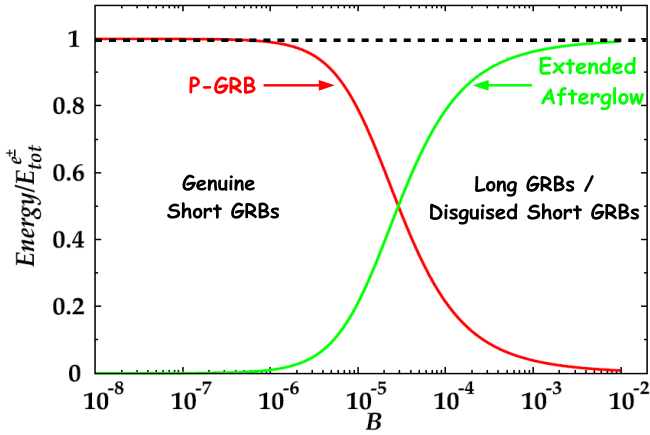


Figure 1. The energy emitted in the extended afterglow (solid green curve) and in the P-GRB (solid red curve) in units of $E_{e^+e^-}^{tot} = 1.77 \times 10^{53}$ erg (dashed horizontal line), as functions of B . The crossing point, corresponding to the condition $E_{P-GRB} \equiv 50\% E_{e^+e^-}^{tot}$, marks the division between the genuine short and disguised short and long GRBs region.

model GRBs originate from an optically thick e^+e^- plasma created by vacuum polarization processes in the gravitational collapse to a black hole (Damour & Ruffini 1975) in the Kerr-Newman geometry (for a recent review see Ruffini et al. 2010). The dynamics of such a plasma in the optically thick phase is described by its total energy $E_{e^+e^-}^{tot}$ and by the amount of the engulfed baryons, Baryon load $B = M_B c^2 / E_{e^+e^-}^{tot}$, where M_B is the mass of the engulfed baryons. The canonical GRBs light curve is characterized by a first emission due to the transparency of the e^+e^- -photon-baryon-plasma, defined as Proper-GRB (P-GRB), followed by an extended afterglow due to the collisions, in a fully radiative regime, between the accelerated baryons and the CBM, with density n_{CBM} (see Sec. 2.1). From these theoretical considerations, it has become clear that the Norris-Bonnell sources belong to a new class of GRBs which have been defined “disguised” short GRBs (Bernardini et al. 2007, 2008; Caito et al. 2009, 2010; de Barros et al. 2011). The initial short spike-like emission is identified as the characteristic emission of the P-GRB. The prolonged soft emission is the extended afterglow occurring in particularly low average density, $\langle n_{CBM} \rangle \approx 10^{-3}$ particles/cm³, typical of a galactic halo environment (see Sec. 2.2).

The aim of this article, using the data obtained by Konus-Wind (Aptekar et al. 1995) and Fermi GBM (Meegan et al. 2009) satellites, is to probe the existence of a yet new class of GRBs which we here define “genuine short GRBs”, theoretically predicted by the Fireshell model (Ruffini et al. 2001b, 2002). This class of canonical GRBs is characterized by severely small values of the Baryon load, $B \lesssim 10^{-5}$ (see Fig. 1). The energy emitted in the P-GRB is predominant and the characteristic duration is expected to be shorter than a fraction of a second (see Sec. 2.3).

We have started a search for these genuine short GRBs among the bursts detected by the Fermi GBM instrument, in its first three years of mission. The initial list of short GRBs was reduced requiring that no prominent X-rays and optical afterglows be observed. From the observed light curves, we have performed the spectral analysis of the source, and within the theory, we have inferred its cosmological redshift, and all the basic parameters of the burst, as well as the isotropic energy, the Lorentz Γ factor at transparency, and the intrinsic duration.

In Sec. 2 we recall the relevant properties of the Fireshell

model. In Sec. 3 we report the observation of GRB 090227B by the different satellites and the data analysis. In Sec. 4 we determine all the quantities of GRB 090227B within the Fireshell scenario, including the redshift. In Sec. 5 we provide an estimation of the lower limit on the Lorentz Γ factor from the definition of opacity, finding the agreement with the theoretically determined Lorentz Γ factor. In the conclusions we show that GRB 090227B is the missing link between the genuine short and the disguised short GRBs, with some common characteristics between the two classes. Further analysis of genuine short GRB with a yet small value of B should lead to P-GRB with a yet more pronounced thermal component. We identify the progenitor of GRB 090227B as a symmetric binary system of two neutron stars, each of $\sim 1.34M_\odot$.

2. REMAINDER OF THE FIRESHELL MODEL

Soon after the announcement of the discovery of GRBs (Strong et al. 1975), Damour & Ruffini (1975) proposed to explain the energy source of GRBs in terms of the e^+e^- pair plasma created in the process of vacuum polarization during the formation of a Kerr-Newman black hole. They mentioned that the energetics to be expected in this model is approximately 10^{54} – 10^{55} ergs for a $10M_\odot$ black hole. At the time nothing was known about the energetics of GRBs, being their distance unknown. They did not pursue further the details of the model pending additional observational evidence.

The idea of the role of an e^+e^- pair plasma as energy source of GRBs was proposed again and independently by Cavallo & Rees (1978). They proposed a sudden release of energy in a process of gravitational collapse leading to a large number of e^+e^- pairs, whose instantaneous annihilation would lead to a vast release of energy pushing on the CBM: the concept of “fireball”.

The concept of fireball was further examined by Goodman (1986), who quantified the dynamical effects of the expansion of such a fireball computing the effect of the blue-shift due to the bulk Lorentz Γ factor on the observed temperature. Shemi & Piran (1990) were among the first to compute the dynamics of such a fireball in presence of baryonic matter, described by the adimensional parameter $\eta = E_0/M_B c^2$, in which E_0 is the initial total energy of the fireball. They clearly pointed out that for large values of η photons carry most of the energy of the fireball. In the opposite regime most of E_0 is converted in the kinetic energy of the baryons and only a small fraction is carried away by the photons at transparency. Further works were presented by Meszaros et al. (1993), Piran et al. (1993) and Katz (1994).

After the discovery by Beppo-SAX (Costa et al. 1997) of the cosmological nature of GRBs, it became clear that the energetics presented by Damour & Ruffini (1975) was indeed correct and their work represented one of the handful GRB models still viable (Ruffini 2001). The return to the model led to a further step in the comprehension of GRBs (Ruffini et al. 1999, 2000) with the detailed analysis of the rate equation which accounts for the gradual annihilation of the pairs, in a relativistic expanding shell, during the entire optically thick acceleration phase of GRBs: the concept of “fireshell”.

The main differences between the fireball and the fireshell scenarios are outlined in the paper of Bianco et al. (2006), while in Aksenov et al. (2007) it was definitely proved that in an optically thick e^+e^- plasma the annihilation of the pairs does not occur instantaneously, as originally assumed by Cavallo and Rees. Instead the optical thick e^+e^- plasma reaches

the thermal equilibrium in a very short time scale, $\sim 10^{-12}$ s, and then dynamically expands following the approach in Ruffini et al. (1999, 2000).

In the meantime the BATSE observations led to a phenomenological classification of GRBs, based on their observed duration, into “long” and “short” GRBs (Klebesadel 1992; Dezalay et al. 1992; Kouveliotou et al. 1993; Tavani 1998). Initially this fact was interpreted in terms of different progenitors for these two classes (see Blinnikov et al. 1984; Woosley 1993; Paczynski 1998).

In 2001 an interpretation within the Fireshell model was proposed to explain the differences between the short and the long GRBs. This interpretation was based on the Baryon load B (inverse of η , see Introduction). In this picture, both long and short GRBs originate from the same basic machine, the dyadotorus, from an implosion leading to the formation of a Kerr-Newman black hole (Ruffini 2009). The long bursts correspond to GRBs with $B \gtrsim 3.0 \times 10^{-4}$ and the short ones to GRBs with $B \lesssim 10^{-5}$ (Fig. 1). For $10^{-5} \lesssim B \lesssim 3.0 \times 10^{-4}$ it depends also on the value of the total energy of the pairs $E_{e^+e^-}^{tot}$ (see below, Fig. 2). The short bursts should have in the limit of $B \rightarrow 0$ no afterglow. This was followed in 2002 by a further theoretical work evidencing also the relevance of an additional parameter influencing the interpretation above classification: the average density of the environment CBM (Ruffini et al. 2002, 2004, 2005b). This led to the new concept of “disguised short” GRBs (Bernardini et al. 2007, 2008; Caito et al. 2009, 2010; de Barros et al. 2011).

Let us briefly go in some more detail in the fireshell model. As we have recalled, the GRBs originate from the process of vacuum polarization occurring in the formation of a black hole, resulting in pair creation (Damour & Ruffini 1975; Ruffini & Xue 2008; Ruffini et al. 2010). The formed e^+e^- plasma, with total energy $E_{e^+e^-}^{tot}$, reaches the thermal equilibrium almost instantaneously (Aksenov et al. 2007). The annihilation of these pairs occurs gradually and it is confined in an expanding shell, called *fireshell*, which self-accelerates up to ultra relativistic velocities (Ruffini et al. 1999), and engulfs the baryonic matter (of mass M_B) left over in the process of collapse, which thermalizes with the pairs due to the large optical depth (Ruffini et al. 2000). The Baryon load is measured by the dimensionless parameter $B = M_B c^2 / E_{e^+e^-}^{tot}$. The fireshell continues to self-accelerate until it reaches the transparency condition and a first flash of radiation, the P-GRB, is emitted (Ruffini et al. 2001b). The radius at which the transparency occurs and the theoretical temperature, the Lorentz factor as well as the amount of the energy emitted in the P-GRB are functions of $E_{e^+e^-}^{tot}$ and B (see Fig. 2). The residual expanding plasma of leptons and baryons interacts with the CBM and, due to these collisions, starts to slow down giving rise to a multi-wavelength emission: the extended afterglow. Assuming a fully-radiative condition, the structures observed in the extended afterglow of a GRB are described by two quantities associated with the environment: the CBM density profile n_{CBM} , which determines the temporal behavior of the light curve, and the fireshell surface filling factor $\mathcal{R} = A_{eff}/A_{vis}$, in which A_{eff} is the effective emitting area of the fireshell and A_{vis} its total visible area (Ruffini et al. 2002, 2005a). This second parameter takes into account the inhomogeneities in the CBM and its filamentary structure (Ruffini et al. 2004). The emission process of the collision between the baryons and the CBM has been assumed in the comoving frame of the shell as a modified black body spectrum (Patricelli et al. 2011), given

by

$$\frac{dN_\gamma}{dV d\epsilon} = \frac{8\pi}{h^3 c^3} \left(\frac{\epsilon}{kT} \right)^\alpha \frac{\epsilon^2}{\exp(\epsilon/kT) - 1}, \quad (1)$$

where α is a phenomenological parameter.

The observed GRB non-thermal spectral shape is then produced by the convolution of a very large number of modified thermal spectra with different temperatures and different Lorentz and Doppler factors. This convolution is performed over the surfaces of constant arrival time for the photons at the detector (EQUiTemporal Surfaces, EQTS, Bianco & Ruffini 2005a,b) encompassing the total observation time. The observed hard-to-soft spectral variation comes out naturally from the decrease with time of the comoving temperature and of the bulk Lorentz Γ factor. This effect is amplified by the curvature effect originated by the EQTS, which produce the observed time lag in the majority of the GRBs.

Assuming the spherical symmetry of the system, the isotropic energy emitted in the burst, E_{iso} , is equal to the energy of the e^+e^- plasma, $E_{e^+e^-}^{tot}$, and the GRB bolometric light curve is composed of the P-GRB and the extended afterglow. Their relative energetics and observed time separation are functions of the energy $E_{e^+e^-}^{tot}$, of the Baryon load B , and of the CBM density distribution n_{CBM} (see Fig. 3). In particular, for B decreasing, the extended afterglow light curve “squeezes” itself on the P-GRB and the P-GRB peak luminosity increases (see Fig. 4).

To reproduce the shape of the light curve we have to determine for each CBM clump the filling factor \mathcal{R} , which determines the effective temperature in the comoving frame and the corresponding peak energy of the spectrum, and of the CBM density n_{CBM} , which determines the temporal behavior of the light curve. It is clear that, since the EQTS encompass emission processes occurring at different comoving times weighted by their Lorentz and Doppler factors, the fit of a single spike is not only a function of the properties of the specific CBM clump but of the entire previous history of the source. Due to the non-linearity of the system and to the EQTS, any change in the simulation produces observable effects up to a much later time. This brings to an extremely complex procedure by trial and error in the data simulation to reach the uniqueness.

2.1. The canonical long GRBs

According to this theory, the canonical long GRBs are characterized by a Baryon load varying in the range $3.0 \times 10^{-4} \lesssim B \leq 10^{-2}$ and they occur in a typical galactic CBM with an average density $\langle n_{CBM} \rangle \approx 1$ particle/cm³. As a result the extended afterglow is predominant with respect to the P-GRB (see Fig. 1).

2.2. The disguised short GRBs

After the observations by Swift of GRB 050509B (Gehrels et al. 2005), which was declared in the literature as the first short GRB with an extended emission ever observed, it has become clear that all such sources are actually disguised short GRBs (de Barros et al. 2011). It is conceivable and probable that also a large fraction of the declared short duration GRBs in the BATSE catalog, observed before the discovery of the afterglow, are members of this class. In the case of the disguised short GRBs the Baryon load varies in the same range of the long bursts, while the CBM density is of the order of 10^{-3} particles/cm³. As a consequence, the extended afterglow results in a “deflated” emission that can be

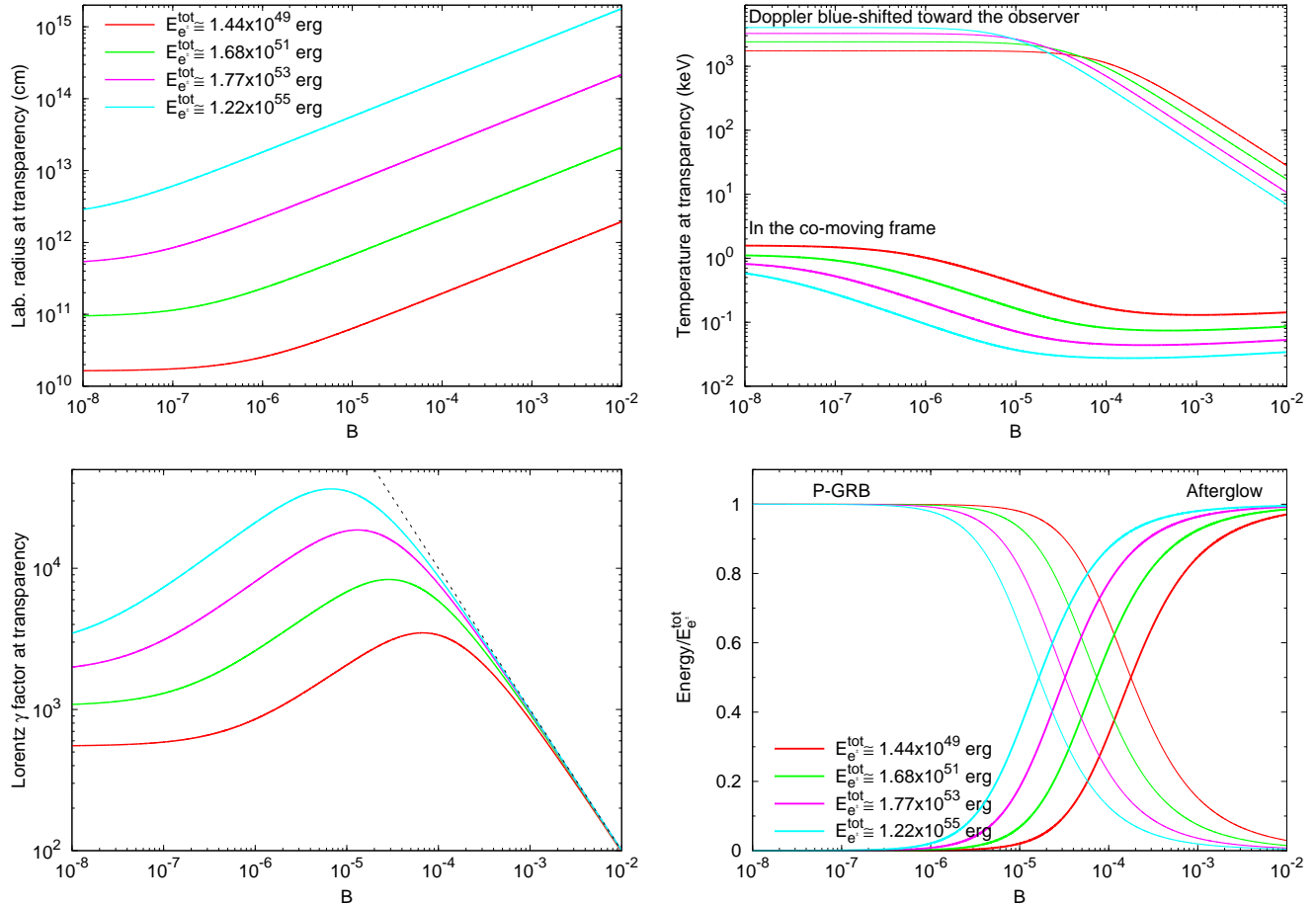


Figure 2. The main quantities of the Fireshell model at the transparency for selected values of $E_{e^-}^{\text{tot}}$: the radius in the laboratory frame, the co-moving frame and blue-shifted toward the observer temperatures of the plasma, the Lorentz Γ factor, and the fraction of energy radiated in the P-GRB and in the extended afterglow as functions of B . In these simulations a sudden transition between the optically thick adiabatic phase and the fully radiative condition at the transparency has been assumed.

exceeded in peak luminosity by the P-GRB (Caito et al. 2009, 2010; de Barros et al. 2011). Indeed the integrated emission in the extended afterglow is much larger than the one of the P-GRB (see Fig. 1), as expected for long GRBs. With these understandings long and disguised short GRBs are interpreted in terms of long GRBs exploding, respectively, in a typical galactic density or in a galactic halo density.

These sources have given the first evidence of GRBs originating from binary mergers, formed by two neutron stars and/or white dwarfs in all possible combinations, that have spiraled out from their host galaxies into the halos (Bernardini et al. 2007, 2008; Caito et al. 2009, 2010; de Barros et al. 2011). This interpretation has been supported by direct optical observations of GRBs located in the outskirts of the host galaxies (Sahu et al. 1997; van Paradijs et al. 1997; Bloom et al. 2006; Troja et al. 2008; Fong et al. 2010; Berger 2011; Kopač et al. 2012).

2.3. The class of genuine short GRBs

In the Fireshell model the genuine short GRBs occur in the limit of very low Baryon load, e.g. $B \lesssim 10^{-5}$ with the P-GRB predominant with respect to the extended afterglow. For such small values of B the afterglow peak emission shrinks over the P-GRB and its flux is lower than the P-GRB one (see Fig. 4).

Since the thermalization of photon-pairs plasma is reached in a very short timescale at the beginning of the expansion

phase and the thermal equilibrium is implemented during the entire phase of the expansion (Aksenov et al. 2007), the spectrum of these genuine short GRBs is expected to be characterized by a significant thermal-like emission. Due to the small values of the Baryon load, in addition to the predominant role of the P-GRB, a non-thermal component originating from the extended afterglow is expected.

3. OBSERVATIONS AND DATA ANALYSIS OF GRB 090227B

At 18:31:01.41 UT on 27th February 2009, the Fermi GBM detector (Guiriec 2009) triggered and located the short and bright burst, GRB 090227B (trigger 257452263/090227772). The on-ground calculated location, using the GBM trigger data, was (RA, Dec)(J2000)=(11^h48^m36^s, 32°10'12''), with an uncertainty of 1.77° (statistical only). The angle from the Fermi LAT boresight was 72°. The burst was also located by IPN (Golenetskii et al. 2009a) and detected by Konus-Wind (Golenetskii et al. 2009b), showing a single pulse with duration ~ 0.2 s (20 keV – 10 MeV). No X rays and optical observations were reported on the GCN Circular Archive, thus the redshift of the source is unknown.

To obtain the Fermi GBM light-curves and the spectrum in the energy range 8 keV – 40 MeV, we made use of the RMFIT program. For the spectral analysis, we have downloaded from the gsfc website⁴ the TTE (Time-Tagged Events) files, suit-

⁴ <ftp://legacy.gsfc.nasa.gov/fermi/data/gbm/bursts>

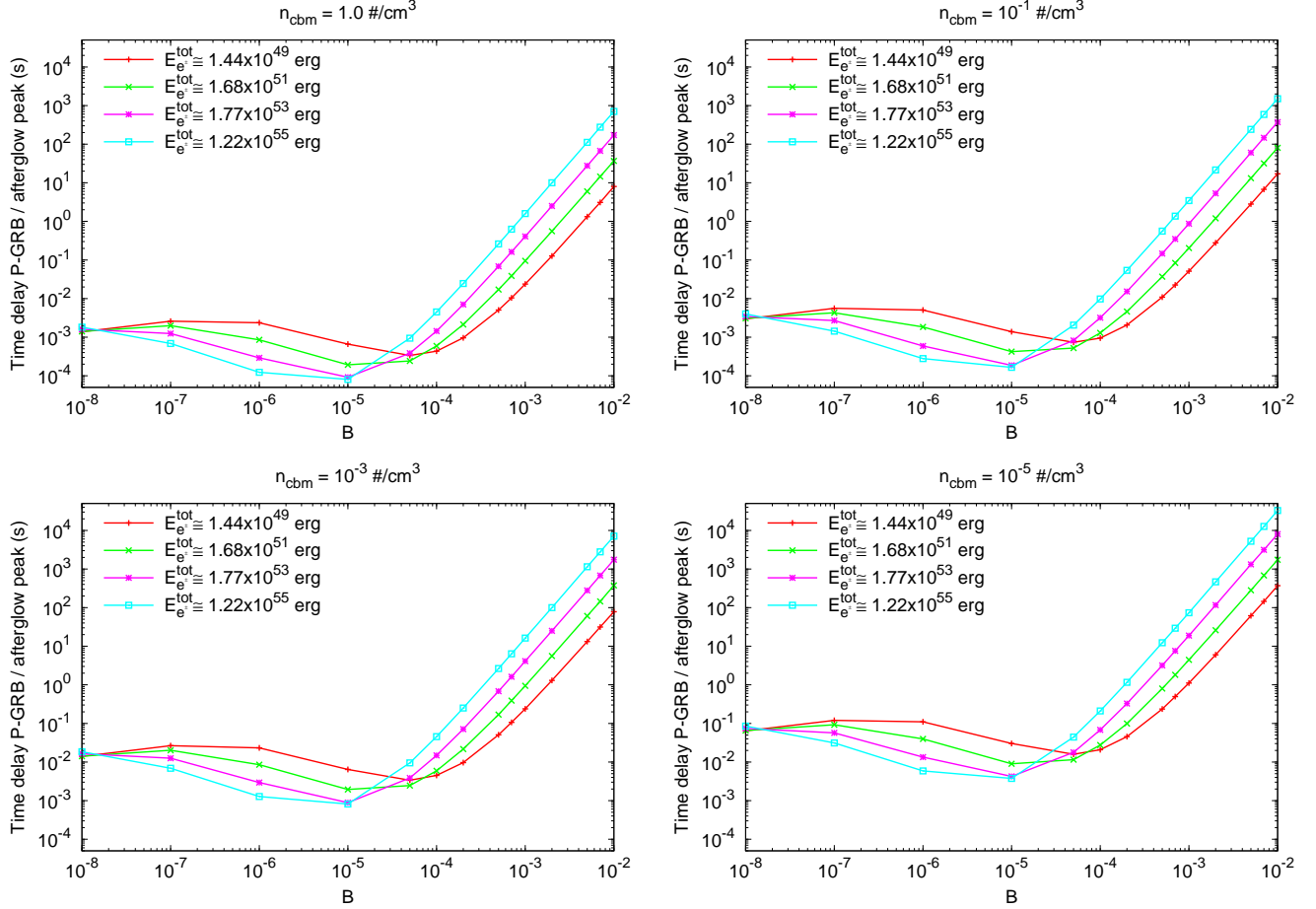


Figure 3. Plots of the arrival time separation Δt_a between the P-GRB and the peak of the extended afterglow as function of B for four different values of $E_{e^+e^-}^{\text{tot}}$, measured in the source cosmological rest frame. This computation has been performed assuming four constant CBM density $n_{\text{CBM}} = 1.0, 1.0 \times 10^{-1}, 1.0 \times 10^{-3}, 1.0 \times 10^{-5}$ particles/cm³.

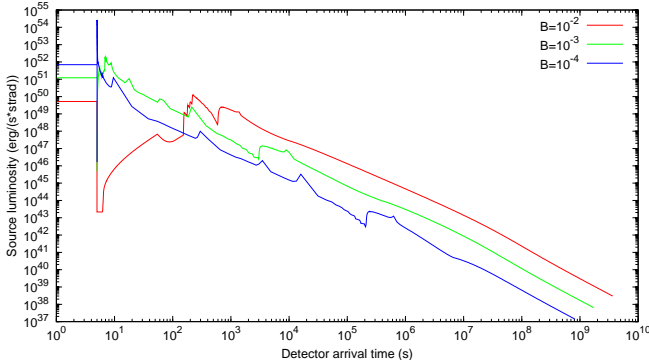


Figure 4. The dependence of the shape of the light curve on B . The computations have been performed assuming $E_{e^+e^-}^{\text{tot}} = 4.83 \times 10^{53}$ ergs, $\langle n_{\text{CBM}} \rangle = 1.0$ particles/cm³, three different values of the Baryon load $B = 10^{-2}, 10^{-3}, 10^{-4}$ and the P-GRBs duration fixed, i.e. 5 s. For B decreasing, the extended afterglow light curve squeezes itself on the P-GRB and the peak becomes sharper and higher.

able for short or highly structured events. We used the light curves corresponding to the NaI-n2 (8 – 900 keV) and the BGO-b0 (250 keV – 40 MeV) detectors. The 64 ms binned GBM light curves show one very bright spike with a short duration of 0.384 s, in the energy range 8 keV – 40 MeV, and a faint tail lasting up to 0.9 s after the trigger time T_0 in the energy range 10 keV – 1 MeV. After the subtraction of the background (fitted by using cubic function), we have proceeded

Spectral Parameter	(-0.064, 0.896)[s]	(-0.064, 0.320)[s]
kT [keV]	397.4 ± 69.6	545.7 ± 36.8
K_{BB} [ph/(cm ² s keV)]	$(2.3 \pm 1.6) \times 10^{-8}$	$(3.11 \pm 1.46) \times 10^{-8}$
α	-0.602 ± 0.050	-0.46 ± 0.04
β	-2.90 ± 0.31	-2.37 ± 0.21
E_{peak} [keV]	1942 ± 249	1252 ± 280
K_{Band} [ph/(cm ² s keV)]	$(4.15 \pm 0.17) \times 10^{-2}$	0.104 ± 0.004
C-STAT/DOF	286.84/240	279.59/238
F_{tot} [erg/(cm ² s)]	$(3.35 \pm 0.12) \times 10^{-5}$	$(8.67 \pm 0.28) \times 10^{-5}$
F_{BB} [erg/(cm ² s)]	$(6.0 \pm 4.2) \times 10^{-6}$	$(2.87 \pm 1.35) \times 10^{-5}$

Table 1

The time-integrated spectral analyses (from $T_0 - 0.064$ s to $T_0 + 0.896$ s, second column, and from $T_0 - 0.064$ s to $T_0 + 0.320$ s, third column) of GRB 090227B performed using BB+Band model in the energy range 8 keV – 40 MeV.

with the time-integrated and time-resolved spectral analyses.

3.1. Time-integrated spectral analysis

We have performed two time-integrated spectral analyses, the first one in the time range from $T_0 - 0.064$ s to $T_0 + 0.896$ s and the second one from $T_0 - 0.064$ s to $T_0 + 0.320$ s, in which we have focused our attention on the spike structure. We have fitted the spectra considering several models and we have found that the best one is a combination of Black Body (BB) and Band (Band et al. 1993) function, with the thermal component superimposed by the non-thermal one (see Fig. 5, right panels). The results of the time-integrated analyses are summarized in Tab. 1.

The Band components are the predominant ones. In fact

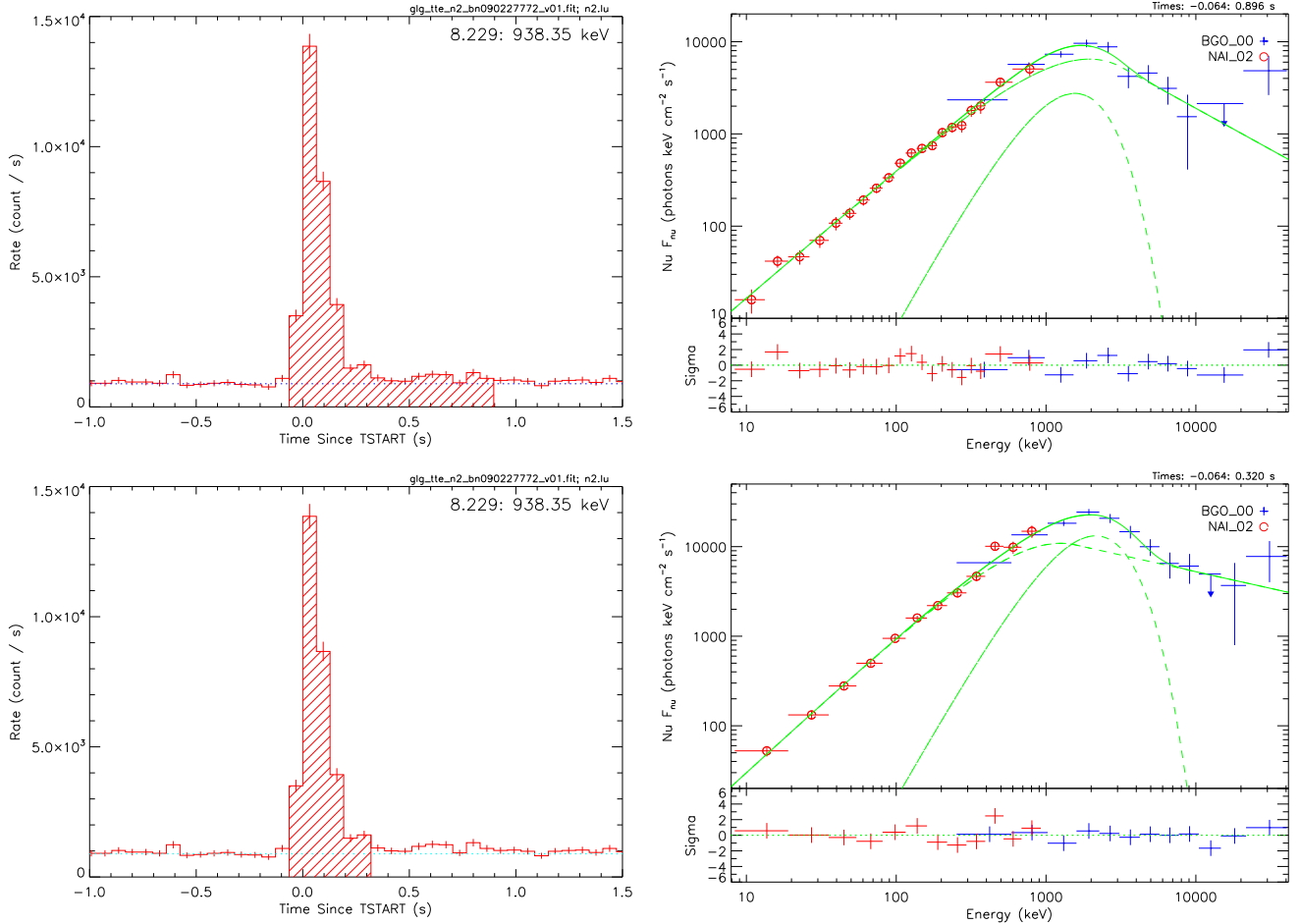


Figure 5. The 64 ms time-binned NaI-n2 light curves (left panels) and the NaI-n2+BGO-b0 νF_ν spectra (right panels) of GRB 090227B in the time intervals from $T_0 - 0.064$ s to $T_0 + 0.896$ s (first row) and from $T_0 - 0.064$ s to $T_0 + 0.320$ s (second row); the best fits show thermal components, superimposed by non thermal ones (in these cases Band spectra).

the ratio between the fluxes of the thermal component and the non-thermal one (NT) is $F_{BB}/F_{NT} \approx 0.22$, in the first time interval, and $F_{BB}/F_{NT} \approx 0.50$, in the second one. However the thermal components have significant weights in the determination of the peaks of the νF_ν spectra, and have the highest temperatures ever observed, respectively, $kT = (397.4 \pm 69.6)$ keV and $kT = (545.7 \pm 36.8)$ keV. Moreover these analyses have revealed that for smaller selected time interval from T_0 the contribution in flux of the thermal component is higher.

From these considerations we have started a time-resolved spectral analysis in order to see if there exists a time interval in which the thermal component becomes predominant and therefore the identification of the P-GRB would be possible.

3.2. Time-resolved spectral analysis

A time-resolved spectral analysis has been performed by Guiriec et al. (2010) by selecting time bins from 2 ms to 94 ms. In view of the low statistical content in these small time bins, the authors fitted the data by using simple Band functions. Instead we have preferred to make an analysis on larger time bins in order to test the presence of BB plus an extra component. The results of this analysis are summarized in Tab. 2.

We have found a significant thermal emission during the early 128 ms. In the remaining ~ 0.8 s there is no evidence of thermal component. Taking advantage of the large statistical

content of each time bin, we have plotted the NaI-n2 light curve of GRB 090227B using time bins of 16 ms (see Fig. 6, left panels). The re-binned light curves show two spike-like substructures. The duration of the first spike is 96 ms and it is clearly distinct from the second spike. In this time range the observed BB temperature is $kT = (517 \pm 28)$ keV (see Tab. 3) and the ratio between the fluxes of the thermal component and the non-thermal one is $F_{BB}/F_{NT} \approx 1.1$. Consequently, we have interpreted the first spike as the P-GRB and the second spike as the extended afterglow. Their spectra are shown in Fig. 6, right panels, and the results of the spectral analysis are summarized in Tab. 3.

4. ANALYSIS OF GRB 090227B IN THE FIRESHIELD MODEL

The identification of the P-GRB is fundamental in order to determine the Baryon load and the other physical quantities characterizing the plasma at the transparency point (see Fig. 2). Crucial is the determination of the cosmological redshift, which can be derived combining the observed fluxes and the spectral properties of the P-GRB and of the extended afterglow with the equation of motion of our theory. From the cosmological redshift we derive $E_{e^+e^-}^{tot}$ and the relative energetics of the P-GRB and of the extended afterglow components (see Fig. 2). Having so derived the Baryon load B and the energy $E_{e^+e^-}^{tot}$, we can constrain the total energy and simulate the canonical light curve of the GRBs with their characteristic pulses, modeled by a variable number density distribution of

t_{start} [s]	t_{stop} [s]	kT [keV]	E_p [keV]	α	β	F_{BB} [erg/cm ² s]	F_{tot} [erg/cm ² s]	χ^2_R	F_{BB}/F_{NT}
-0.032	0.000	199 ± 14	...	-1.462 ± 0.081	...	$(4.09 \pm 0.94) \times 10^{-5}$	$(7.4 \pm 1.3) \times 10^{-5}$	0.94	1.25
0.000	0.032	651 ± 70	1121 ± 402	-0.08 ± 0.14	-1.462 ± 0.081	$(2.9 \pm 1.8) \times 10^{-4}$	$(4.66 \pm 0.21) \times 10^{-4}$	1.01	1.64
0.032	0.064	438 ± 21	...	-1.118 ± 0.030	...	$(1.97 \pm 0.29) \times 10^{-4}$	$(4.66 \pm 0.33) \times 10^{-4}$	1.03	0.73
0.064	0.096	334 ± 20	...	-1.404 ± 0.045	...	$(9.2 \pm 1.8) \times 10^{-5}$	$(1.83 \pm 0.19) \times 10^{-4}$	1.02	1.02
0.096	0.128	136 ± 11	...	-1.226 ± 0.034	...	$(2.89 \pm 0.78) \times 10^{-5}$	$(2.23 \pm 0.26) \times 10^{-4}$	1.07	0.15
0.128	0.160	35.5 ± 4.8	...	-1.516 ± 0.080	...	$(3.3 \pm 1.7) \times 10^{-6}$	$(2.87 \pm 0.95) \times 10^{-5}$	0.84	0.13
0.160	0.192	24.1 ± 8.6	...	-1.252 ± 0.077	...	unconstrained	$(7.1 \pm 1.5) \times 10^{-5}$	0.90	< 0.01

Table 2

Time-resolved analysis of GRB 090227B. In the first two columns we have indicated the time bin and in the third one the temperature of the thermal component; in the following three columns we have summarized the parameters of the non-thermal component [in all the time bins a simple power-law (PL), with the exception of the second one in which we have a Band function]. In the last four columns we have respectively the flux of the BB component, the total flux, the reduced- χ^2 , and the ratio between the thermal and the non-thermal fluxes.

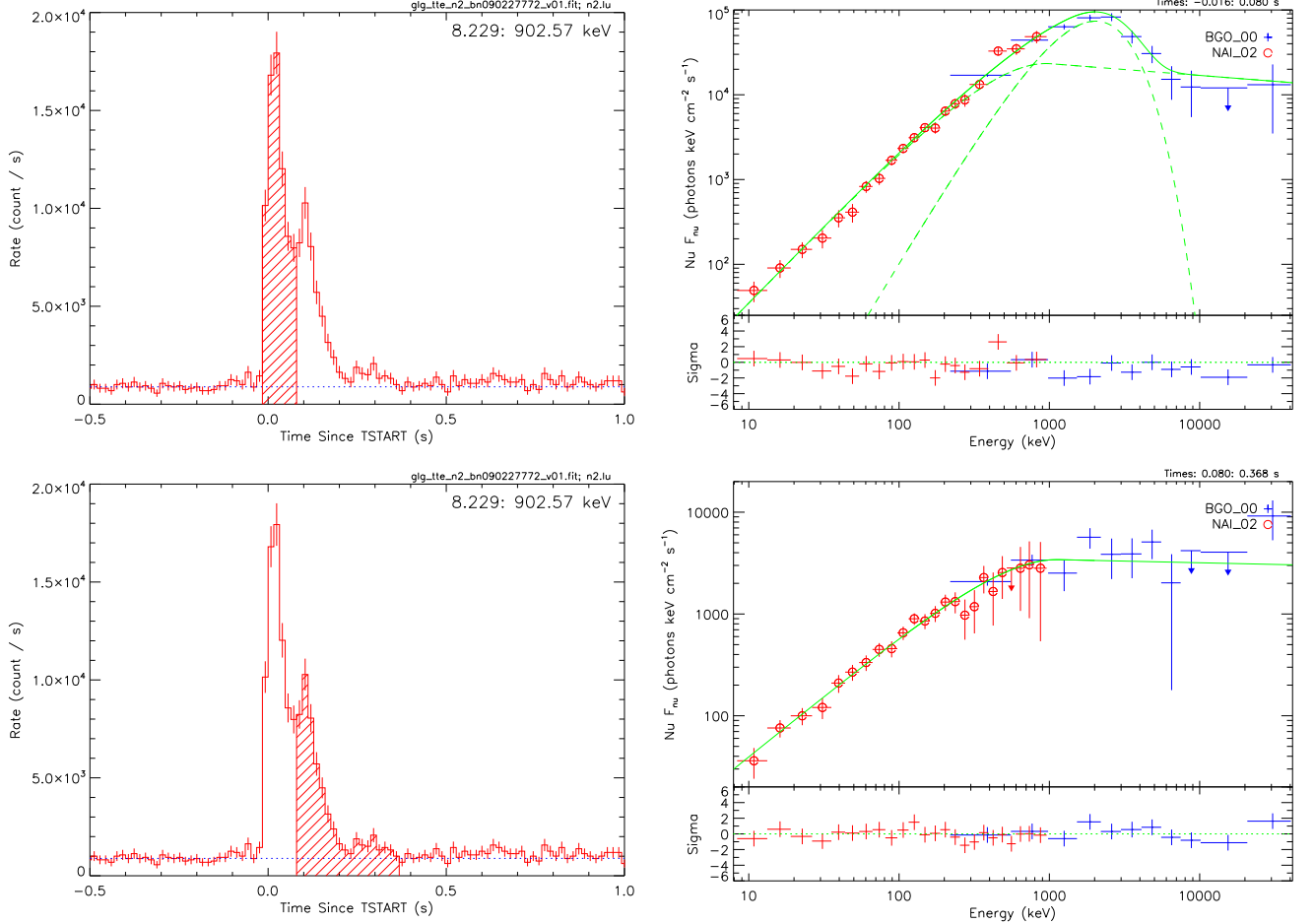


Figure 6. The 16 ms time-binned NaI-n2 light curves of the P-GRB (left upper panel) and the extended afterglow (left lower panel) and their NaI-n2+BGO-b0 νF_ν spectra (on the right, the upper panel for the P-GRB and the lower one for the extended afterglow). Also in this case the best fit of the P-GRB is composed of a BB superimposed by a Band spectrum; the best fit of the extended afterglow is a simple Band function.

Spectral Parameter	P-GRB	Extended Afterglow
kT [keV]	517 ± 28	...
K_{BB} [ph/(cm ² s keV)]	$(2.16 \pm 0.63) \times 10^{-7}$...
α	-0.18 ± 0.11	-0.801 ± 0.054
β	-2.14 ± 0.17	-2.03 ± 0.11
E_{peak} [keV]	952 ± 251	1113 ± 188
K_{Band} [ph/(cm ² s keV)]	0.237 ± 0.021	$(6.31 \pm 0.33) \times 10^{-2}$
C-STAT/DOF	263.51/239	271.73/242
F_{tot} [erg/(cm ² s)]	$(3.13 \pm 0.13) \times 10^{-4}$	$(2.68 \pm 0.26) \times 10^{-5}$
F_{BB} [erg/(cm ² s)]	$(1.61 \pm 0.47) \times 10^{-4}$...

Table 3

The results of the spectral analysis of the P-GRB (from $T_0 - 0.016$ s to $T_0 + 0.080$ s, best fit BB+Band model) and the extended afterglow (from $T_0 + 0.080$ s to $T_0 + 0.368$ s, best fit Band model) of GRB 090227B in the energy range 8 keV – 40 MeV.

the CBM around the burst site.

4.1. Estimation of the redshift of GRB 090227B

Having determined the redshift of the source, the analysis consists of equating $E_{e^+e^-}^{tot} \equiv E_{iso}$ (namely E_{iso} is a lower limit on $E_{e^+e^-}^{tot}$) and inserting a value of the Baryon load to complete the simulation. The right set of $E_{e^+e^-}^{tot}$ and B is determined when the theoretical energy and temperature of the P-GRB match the observed ones of the thermal emission [namely $E_{P-GRB} \equiv E_{BB}$ and $kT_{obs} = kT_{blue}/(1+z)$].

In the case of GRB 090227B we have estimated the ratio $E_{P-GRB}/E_{e^+e^-}^{tot}$ from the observed fluences

$$\frac{E_{P-GRB}}{E_{e^+e^-}^{tot}} = \frac{4\pi d_1^2 F_{BB} \Delta t_{BB} / (1+z)}{4\pi d_1^2 F_{tot} \Delta t_{tot} / (1+z)} = \frac{S_{BB}}{S_{tot}}, \quad (2)$$

Fireshell Parameter	Value
$E_{e^+e^-}^{tot}$ [erg]	$(2.83 \pm 0.15) \times 10^{53}$
B	$(4.13 \pm 0.05) \times 10^{-5}$
Γ_{tr}	14365
r_{tr} [cm]	1.76×10^{13}
kT_{blue} [keV]	1336
z	1.61 ± 0.14
$\langle n \rangle$ [particles/cm ³]	1.90×10^{-5}
$\langle \delta n/n \rangle$	0.82

Table 4

The results of the simulation of GRB 090227B in the Fireshell model. The parameters with the errors follow directly from the observation, while the fixed ones from the theory.

where d_l is the luminosity distance of the source and $S = F \Delta t$ are the fluences. The BB fluence is $S_{BB} = (1.54 \pm 0.45) \times 10^{-5}$ erg/cm², while the total fluence (from $T_0 - 0.016$ to $T_0 + 0.896$ s) is $S_{tot} = (3.79 \pm 0.20) \times 10^{-5}$ erg/cm². Therefore the observed energy ratio is $E_{P-GRB}/E_{e^+e^-}^{tot} = (40.67 \pm 0.12)\%$. As is clear from the bottom right diagram in Fig. 2, for each value of this ratio we have a range of possible parameters B and $E_{e^+e^-}^{tot}$. In turn, for each value of them we can determine the theoretical blue-shifted toward the observer temperature kT_{blue} (see top right diagram in Fig. 2). Correspondingly, for each couple of value of B and $E_{e^+e^-}^{tot}$ we estimate the value of z by the ratio between kT_{blue} and the observed temperature of the P-GRB kT_{obs} ,

$$\frac{kT_{blue}}{kT_{obs}} = 1 + z. \quad (3)$$

In order to remove the degeneracy $[E_{e^+e^-}^{tot}(z), B(z)]$, we have made use of the isotropic energy formula

$$E_{iso} = 4\pi d_l^2 \frac{S_{tot}}{(1+z)} \frac{\int_{E_{min}/(1+z)}^{E_{max}/(1+z)} EN(E)dE}{\int_8^{40000} EN(E)dE}, \quad (4)$$

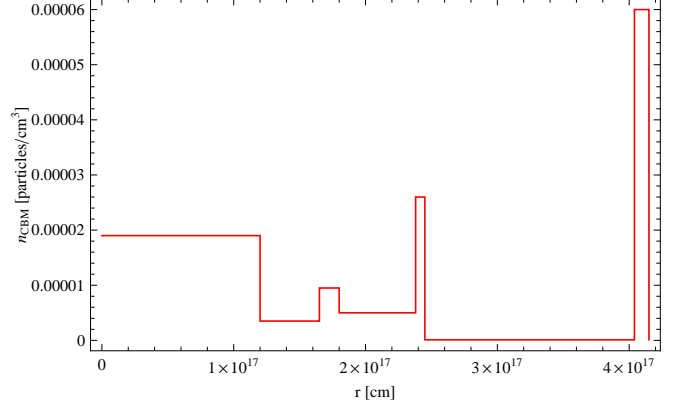
in which $N(E)$ is the photon spectrum of the burst and the integrals are due to the bolometric correction on S_{tot} . The correct value is the one for which the condition $E_{iso} \equiv E_{e^+e^-}^{tot}$ is satisfied.

We have found the equality at $z = 1.61 \pm 0.14$ for $B = (4.13 \pm 0.05) \times 10^{-5}$ and $E_{e^+e^-}^{tot} = (2.83 \pm 0.15) \times 10^{53}$ ergs. The complete quantities so determined are summarized in the Tab. 4.

4.2. The analysis of the extended afterglow and the observed spectrum of the P-GRB

As recalled in Sec. 2, the arrival time separation between the P-GRB and the peak of the extended afterglow is a function of $E_{e^+e^-}^{tot}$ and B and depends on the detailed profile of the CBM density. For $B \sim 4 \times 10^{-5}$ (see Fig. 3) the time separation is $\sim 10^{-3} - 10^{-2}$ s in the source cosmological rest frame. In this light, there is an interface between the reaching of transparency of the P-GRB and the early part of the extended afterglow. This connection has already been introduced in literature (Pe'er et al. 2010; Izzo et al. 2012; Penacchioni et al. 2012).

The determination of the above quantities leads to the initial value of the Lorentz Γ factor of $\Gamma_{tr} = 14365$. We have simulated the light curve of the extended afterglow by defining the radial distribution of the CBM around the burst site, which is shown in Fig. 7, and it is characterized by a mean value $\langle n \rangle = 1.90 \times 10^{-5}$ particles/cm³ and an average density

**Figure 7.** The radial CBM density distribution of GRB 090227B.

contrast $\langle \delta n/n \rangle = 0.82$ (see also Tab. 4). These values are typical of the galactic halos environment. The filling factor varies in the range $9.1 \times 10^{-12} \leq \mathcal{R} \leq 1.5 \times 10^{-11}$, up to 2.38×10^{17} cm away from the burst site, and then drops to the value $\mathcal{R} = 1.0 \times 10^{-15}$. The value of the α parameter has been found to be -1.99 along the total duration of the GRB. In Fig. 8 we show the simulated light curve (8–1000 keV) of GRB 090227B and the corresponding spectrum in the early ~ 0.4 s of the emission, using the spectral model described in Bianco & Ruffini (2004) and Patricelli et al. (2011).

We turn now to the emission of the early 96 ms. We have studied the interface between the P-GRB emission and the onset of the extended afterglow emission. In Fig. 9 we have plotted the thermal spectrum of the P-GRB and the Fireshell simulation (from $T_0 + 0.015$ s to $T_0 + 0.080$ s) of the early interaction of the extended afterglow. The sum of these two components is compared with the observed spectrum in Fig. 9.

5. CONSISTENCY WITH THE OPACITY DUE TO PAIR PRODUCTION

It is interesting to compare the Lorentz Γ factor theoretically determined with the lower limit coming from the opacity argument.

An estimate on this lower limit comes out from the solution of the classical compactness problem for GRBs which arises from the combination of their large energy released, $\sim 10^{51}$ ergs, the short time scale δt of a few milliseconds and the observed hard non-thermal spectrum. Using the usual (Newtonian) causality limit on the size $R \leq c\delta t$ to estimate the density of photons, one finds that the optical depth for pair production at the source $\gamma\gamma \rightarrow e^+e^-$ would be $\sim 10^{15}$ (see Piran 1999). Such an optically thick source could not emit the observed non-thermal spectrum.

As Ruderman (1975) pointed out, relativistic effects can resolve this problem. The causality limit of a source moving relativistically with Lorentz factor $\Gamma \gg 1$ towards us is $R \leq c\delta t/\Gamma^2$. Additionally the observed photons have been blue-shifted. At the source they have lower energy, by a factor $\approx 1/\Gamma$, which may be insufficient for pair production. Together this leads to a decrease in the estimated optical depth by a factor $\Gamma^{2+2\beta}$ (Piran 2012), where β is the high energy spectral index of the photon number distribution. Thus, the average optical depth, up to a factor due to the cosmological effects, is

$$\tau_{\gamma\gamma} = \frac{f_p}{\Gamma^{2+2\beta}} \frac{\sigma_T S d_l^2}{c^2 \delta t^2 m_e c^2}, \quad (5)$$

where f_p is the fraction of photon pairs at the source that can

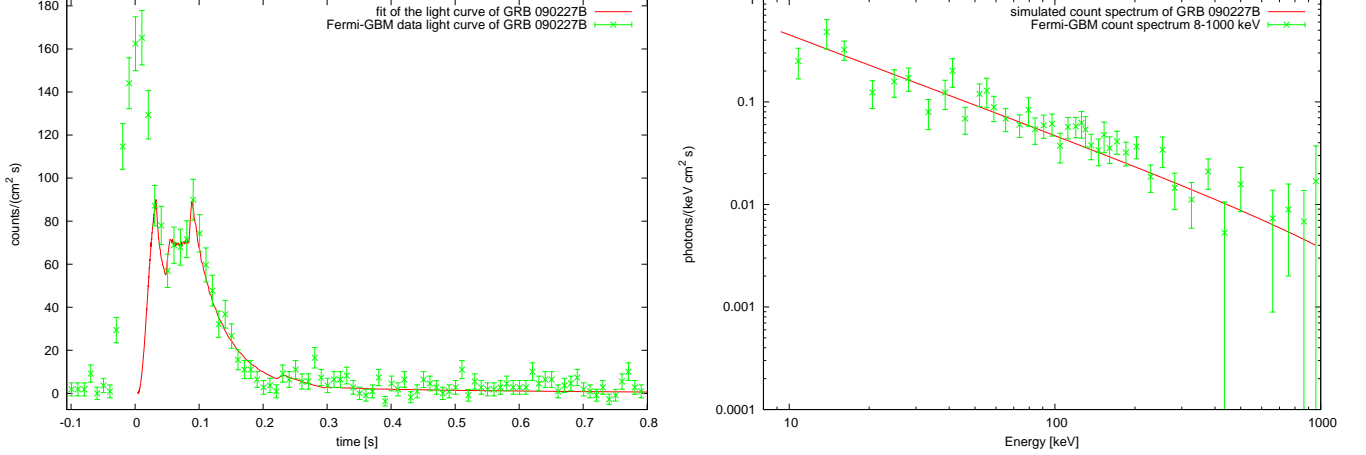


Figure 8. The simulated light curve and the time-integrated (from $T_0 + 0.015$ s to $T_0 + 0.385$ s) photon number spectrum in the energy band 8–1000 keV of the extended-afterglow of GRB 090227B.

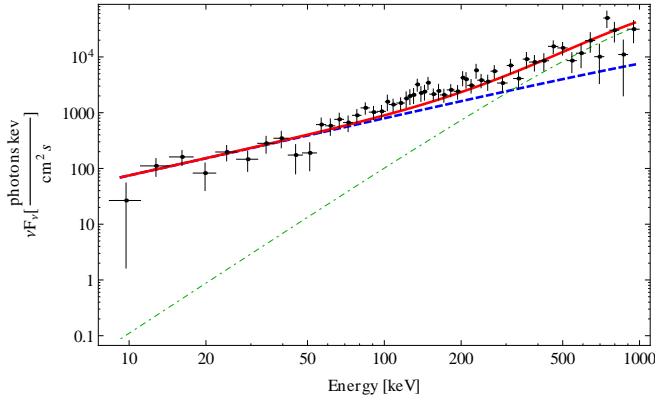


Figure 9. The time-integrated (from $T_0 + 0.015$ s to $T_0 + 0.080$ s) Fireshell simulation in the energy band 8–1000 keV, dashed blue line, and the BB emission, dashed-dotted green line. The sum of the two components, the solid red line, is compared to the observed P-GRB emission.

effectively produce pairs, σ_T is the Thompson cross-section and S is the observed fluence. For $\tau_{\gamma\gamma} < 1$, by setting δt equal to minimum variability time scale observed for GRB 090227B, ~ 2 ms (Guiriec et al. 2010), and using the observed total fluence, $S_{tot} = 3.79 \times 10^{-5}$ erg/cm², and the theoretically inferred redshift, $z = 1.61$, we obtain a lower limit $\Gamma > 594$.

We can conclude that the Lorentz factor at the transparency theoretically derived from the Fireshell equation of motion is consistent with this lower value.

6. CONCLUSIONS

GRB 090227B is the prototype of the class of “genuine short GRBs” with the Baryon load $B \lesssim 5 \times 10^{-5}$, theoretically predicted by the Fireshell model (Ruffini et al. 2001a,b,c).

From the observations, GRB 090227B has an overall emission lasting ~ 0.9 s with a fluence of 3.79×10^{-5} erg/cm² in the energy range 8 keV – 40 MeV. In absence of an optical identification, no determination of its cosmological redshift and of its energetics was possible.

Thanks to the excellent data available from Fermi-GBM (Meegan et al. 2009) and Konus-Wind (Aptekar et al. 1995), it has been possible to probe the comparison between the observation and the theoretical model.

A detailed spectral analysis on the time scale as short as 16 ms has led to identify a thermal emission. We have iden-

tified this emission with the theoretically expected P-GRB component and the remaining part as the extended afterglow. Consequently, we have determined the cosmological redshift, $z = 1.61$, as well as the Baryon load, $B = 4.13 \times 10^{-5}$, its energetics, $E_{e^+e^-}^{tot} = 2.83 \times 10^{53}$ ergs, and the extremely high Lorentz Γ factor at the transparency, $\Gamma_{tr} = 14365$.

We are led to the conclusion (see also Rueda & Ruffini 2012) that the progenitor of this GRB is a binary neutron star, which for simplicity we assume to have the same mass, by the following considerations:

1. the very low average number density of the CBM, $\langle n_{CBM} \rangle \sim 10^{-5}$ particles/cm³; this fact points to two compact objects in a binary system that have spiraled out in the halo of their host galaxy (see Bernardini et al. 2007, 2008; Bianco et al. 2008; Caito et al. 2009, 2010; de Barros et al. 2011);
2. the large total energy, $E_{e^+e^-}^{tot} = 2.83 \times 10^{53}$ ergs, which we can indeed infer in view of the absence of beaming, and the very short time scale of emission point again to two neutron stars. In light of the recent neutron star theory in which all the fundamental interactions are taken into account (Belvedere et al. 2012), we are led to a binary neutron star with masses $m_1 = m_2 = 1.34M_\odot$, radii $R_1 = R_2 = 12.24$ km, and, consequently, total mass $m_1 + m_2$ larger than the critical mass, $2.67M_\odot$;
3. the very small value of the Baryon load, $B = 4.13 \times 10^{-5}$, is consistent with two neutron stars with crusts of ~ 0.47 km of thickness. The new theory of the neutron stars, developed in Belvedere et al. (2012), leads to the prediction of GRBs with still smaller Baryon load and, consequently, shorter periods. We indeed infer an absolute upper limit on the energy emitted via gravitational waves, $\sim 9.6 \times 10^{52}$ ergs (see Rueda & Ruffini 2012).

We can then generally conclude on the existence of three different possible structures of the canonical GRBs (see Fig. 10 and Tab. 5):

- a. long GRB with Baryon load $3.0 \times 10^{-4} \lesssim B \leq 10^{-2}$, exploding in a CBM with average density of $\langle n_{CBM} \rangle \approx 1$ particle/cm³, typical of the inner galactic regions;
- b. disguised short GRBs with the same Baryon load as the previous class, but occurring in a CBM with

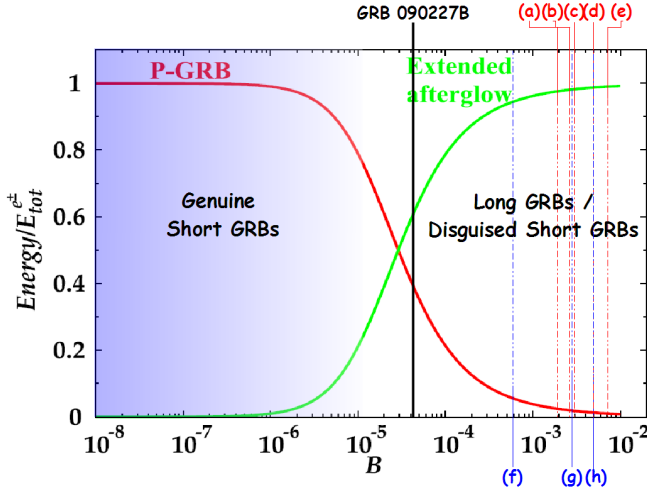


Figure 10. The energy emitted in the extended afterglow (green curve) and in the P-GRB (red curve) in units of the total energy $E_{e^+e^-}^{tot} = 1.77 \times 10^{53}$ erg are plotted as functions of the B parameter. In the figure are also marked some values of the Baryon load: in black GRB 090227B and in red and blue some values corresponding to, respectively, some long and disguised short GRBs we analyzed.

label	GRB	$E_{e^+e^-}^{tot}$ [erg]	B	$\langle n_{CBM} \rangle$ [#cm ³]
(a)	090618	2.49×10^{53}	1.98×10^{-3}	1.0
(b)	080319B	1.32×10^{54}	2.50×10^{-3}	6.0
(c)	991216	4.83×10^{53}	3.00×10^{-3}	1.0
(d)	030329	2.12×10^{52}	4.80×10^{-3}	2.0
(e)	031203	1.85×10^{50}	7.40×10^{-3}	0.3
(f)	050509B	5.52×10^{48}	6.00×10^{-4}	1.0×10^{-3}
(g)	060614	2.94×10^{51}	2.80×10^{-3}	1.0×10^{-3}
(h)	970228	1.45×10^{54}	5.00×10^{-3}	9.5×10^{-4}
	090227B	2.83×10^{53}	4.13×10^{-5}	1.9×10^{-5}

Table 5

List of the long and disguised short GRBs labeled in Fig.10 with in addition GRB 090227B. For each burst the total energy of the plasma, the Baryon load, and the average CBM density are indicated.

$\langle n_{CBM} \rangle \approx 10^{-3}$ particle/cm³, typical of galactic halos (Bernardini et al. 2007, 2008; Bianco et al. 2008; Caito et al. 2009, 2010; de Barros et al. 2011);

- c. genuine short GRBs which occur for $B \lesssim 10^{-5}$ with the P-GRB predominant with respect to the extended afterglow and exploding in a CBM with $\langle n_{CBM} \rangle \approx 10^{-5}$ particle/cm³, typical again of galactic halos, being GRB 090227B the first prototype.

Both classes of GRBs occurring in galactic halos originate from binary mergers.

REFERENCES

- Aksenov, A. G., Ruffini, R., & Vereshchagin, G. V. 2007, Physical Review Letters, 99, 125003
- Aptekar, R. L., Frederiks, D. D., Golenetskii, S. V., et al. 1995, Space Sci. Rev., 71, 265
- Band, D., Matteson, J., Ford, L., et al. 1993, ApJ, 413, 281
- Belvedere, R., Pugliese, D., Rueda, J. A., Ruffini, R., & Xue, S.-S. 2012, Nuclear Physics A, 883, 1
- Berger, E. 2011, New Astron. Rev., 55, 1
- Bernardini, M. G., Bianco, C. L., Caito, L., et al. 2007, A&A, 474, L13
- Bernardini, M. G., Bianco, C. L., Caito, L., et al. 2008, in American Institute of Physics Conference Series, Vol. 966, Relativistic Astrophysics, ed. C. L. Bianco & S. S. Xue, 7–11
- Bianco, C. L., Bernardini, M. G., Caito, L., et al. 2008, in American Institute of Physics Conference Series, Vol. 966, Relativistic Astrophysics, ed. C. L. Bianco & S. S. Xue, 12–15
- Bianco, C. L., & Ruffini, R. 2004, ApJ, 605, L1
- . 2005a, ApJ, 633, L13
- . 2005b, ApJ, 620, L23
- Bianco, C. L., Ruffini, R., Vereshchagin, G. V., & Xue, S. 2006, Journal of the Korean Physical Society, 49, 722
- Blinnikov, S. I., Novikov, I. D., Perevodchikova, T. V., & Polnarev, A. G. 1984, Soviet Astronomy Letters, 10, 177
- Bloom, J. S., Prochaska, J. X., Pooley, D., et al. 2006, ApJ, 638, 354
- Caito, L., Amati, L., Bernardini, M. G., et al. 2010, A&A, 521, A80+
- Caito, L., Bernardini, M. G., Bianco, C. L., et al. 2009, A&A, 498, 501
- Cavallo, G., & Rees, M. J. 1978, MNRAS, 183, 359
- Costa, E., Frontera, F., Heise, J., et al. 1997, Nature, 387, 783
- Damour, T., & Ruffini, R. 1975, Physical Review Letters, 35, 463
- de Barros, G., Amati, L., Bernardini, M. G., et al. 2011, A&A, 529, A130
- Dezalay, J.-P., Barat, C., Talon, R., et al. 1992, in American Institute of Physics Conference Series, Vol. 265, American Institute of Physics Conference Series, ed. W. S. Paciesas & G. J. Fishman, 304–309
- Fong, W., Berger, E., & Fox, D. B. 2010, ApJ, 708, 9
- Gehrels, N., Sarazin, C. L., O’Brien, P. T., et al. 2005, Nature, 437, 851
- Golenetskii, S., Aptekar, R., Mazets, E., et al. 2009a, GRB Coordinates Network, 8925, 1
- . 2009b, GRB Coordinates Network, 8926, 1
- Goodman, J. 1986, ApJ, 308, L47
- Guiriec, S. 2009, GRB Coordinates Network, 8921, 1
- Guiriec, S., Briggs, M. S., Connaughton, V., et al. 2010, ApJ, 725, 225
- Izzo, L., Ruffini, R., Penacchioni, A. V., et al. 2012, ArXiv e-prints
- Katz, J. I. 1994, ApJ, 422, 248
- Klebesadel, R. W. 1992, in Gamma-Ray Bursts - Observations, Analyses and Theories, ed. C. Ho, R. I. Epstein, & E. E. Fenimore (Cambridge University Press), 161–168
- Kopač, D., D’Avanzo, P., Melandri, A., et al. 2012, ArXiv e-prints
- Kouveliotou, C., Meegan, C. A., Fishman, G. J., et al. 1993, ApJ, 413, L101
- Meegan, C., Lichti, G., Bhat, P. N., et al. 2009, ApJ, 702, 791
- Meegan, C. A., Fishman, G. J., Wilson, R. B., et al. 1992, Nature, 355, 143
- Meszáros, P., Laguna, P., & Rees, M. J. 1993, ApJ, 415, 181
- Metzger, M. R., Djorgovski, S. G., Kulkarni, S. R., et al. 1997, Nature, 387, 878
- Norris, J. P., & Bonnell, J. T. 2006, ApJ, 643, 266
- Paczynski, B. 1998, ApJ, 494, L45
- Patricelli, B., Bernardini, M. G., Bianco, C. L., et al. 2011, International Journal of Modern Physics D, 20, 1983
- Pe’er, A., Zhang, B.-B., Ryde, F., et al. 2010, ArXiv e-prints
- Penacchioni, A. V., Ruffini, R., Izzo, L., et al. 2012, A&A, 538, A58
- Piran, T. 1999, Phys. Rep., 314, 575
- Piran, T. 2012, in Twelfth Marcel Grossmann Meeting on General Relativity, 269
- Piran, T., Shemi, A., & Narayan, R. 1993, MNRAS, 263, 861
- Ruderman, M. 1975, in Annals of the New York Academy of Sciences, Vol. 262, Seventh Texas Symposium on Relativistic Astrophysics, ed. P. G. Bergman, E. J. Fenyves, & L. Motz, 164–180
- Rueda, J. A., & Ruffini, R. 2012, Phys. Rev. Lett. (submitted to)
- Ruffini, R. 2001, in Fluctuating Paths and Fields, ed. W. Janke, A. Pelster, H. J. Schmidt, & M. Bachmann (Singapore: World Scientific)
- Ruffini, R. 2009, in The Kerr Spacetime, ed. D. L. Wiltshire, M. Visser, & S. Scott (Cambridge University Press)
- Ruffini, R., Bernardini, M. G., Bianco, C. L., et al. 2005a, in American Institute of Physics Conference Series, Vol. 782, XIth Brazilian School of Cosmology and Gravitation, ed. M. Novello & S. E. Perez Bergliaffa, 42
- Ruffini, R., Bianco, C. L., Chardonnet, P., Frascchetti, F., & Xue, S. 2002, ApJ, 581, L19
- Ruffini, R., Bianco, C. L., Frascchetti, F., Xue, S.-S., & Chardonnet, P. 2001a, ApJ, 555, L117
- . 2001b, ApJ, 555, L113
- . 2001c, ApJ, 555, L107
- Ruffini, R., Bianco, C. L., Xue, S.-S., et al. 2004, International Journal of Modern Physics D, 13, 843
- . 2005b, International Journal of Modern Physics D, 14, 97
- Ruffini, R., Salmonson, J. D., Wilson, J. R., & Xue, S. 2000, A&A, 359, 855
- Ruffini, R., Salmonson, J. D., Wilson, J. R., & Xue, S.-S. 1999, A&A, 350, 334
- Ruffini, R., Vereshchagin, G., & Xue, S.-S. 2010, Phys. Rep., 487, 1
- Ruffini, R., & Xue, S.-S. 2008, in American Institute of Physics Conference Series, Vol. 1059, American Institute of Physics Conference Series, ed. D.-S. Lee & W. Lee, 72–100
- Sahu, K. C., Livio, M., Petro, L., et al. 1997, Nature, 387, 476
- Shemi, A., & Piran, T. 1990, ApJ, 365, L55

Strong, I. B., Klebesadel, R. W., & Evans, W. D. 1975, in *Annals of the New York Academy of Sciences*, Vol. 262, Seventh Texas Symposium on Relativistic Astrophysics, ed. P. G. Bergman, E. J. Fenyves, & L. Motz, 145–158
Tavani, M. 1998, *ApJ*, 497, L21

Tavani, M., Argan, A., Barbiellini, G., et al. 2008, in *American Institute of Physics Conference Series*, Vol. 1000, American Institute of Physics Conference Series, ed. M. Galassi, D. Palmer, & E. Fenimore, 523–530
Troja, E., King, A. R., O'Brien, P. T., Lyons, N., & Cusumano, G. 2008, *MNRAS*, 385, L10
van Paradijs, J., Groot, P. J., Galama, T., et al. 1997, *Nature*, 386, 686
Woosley, S. E. 1993, *ApJ*, 405, 273